Time-Resolved PIV for Space-Time Correlations in Hot Jets

Mark P. Wernet
NASA Glenn Research Center
Cleveland, OH 44135 USA

Abstract- **Temporally Resolved Particle Image Velocimetry (TR-PIV) is being used to characterize the decay of turbulence in jet flows – a critical element for understanding the acoustic properties of the flow. A TR-PIV system, developed in-house at the NASA Glenn Research Center, is capable of acquiring planar PIV image frame pairs at up to 10 kHz. The data reported here were collected at Mach numbers of 0.5 and 0.9 and at temperature ratios of 0.89 and 1.76. The field of view of the TR-PIV system covered 6 nozzle diameters along the lip line of the 50.8 mm diameter jet. The cold flow data at Mach 0.5 were compared with hotwire anemometry measurements in order to validate the new TR-PIV technique. The axial turbulence profiles measured across the shear layer using TR-PIV were thinner than those measured using hotwire anemometry and remained centered along the nozzle lip line. The collected TR-PIV data illustrate the differences in the single point statistical flow properties of cold and hot jet flows. The planar, time-resolved velocity records were then used to compute two-point space-time correlations of the flow at the Mach 0.9 flow condition. The TR-PIV results show that there are differences in the convective velocity and growth rate of the turbulent structures between cold and hot flows at the same Mach number.**

I. INTRODUCTION

Particle Image Velocimetry (PIV) has developed into a production grade research tool, which has been used in a wide variety of applications. At the NASA Glenn Research Center (GRC), PIV has been extensively used to characterize the first and second order statistical properties of both cold and hot jet flows from internally and externally mixed nozzles in the Nozzle Acoustic Test Rig (NATR) [1] and from simple and chevron equipped nozzles in the Small Hot Jet Acoustics Rig (SHJAR) [2]. These PIV measurements provide an extensive and accurate database of 1st and 2nd order statistics for validation of Computational AeroAcoustic codes (CAA). The accuracy of these aeroacoustic models is directly dependent on our ability to accurately characterize turbulent flow statistics. The Lighthill acoustic analogy yields a fourth order two-point space-time correlation, which has previously proved difficult or impossible to measure in hot flows [3]. The need for two-point space-time correlation measurements of hot jet flows is widely recognized in the aeroacoustic community, since it is the pathway for determining the noise source terms [4]. Use of traditional hotwire probes in these hot jet flow fields is precluded due to the compressibility effects and elevated temperatures. Hence, a non-intrusive means for measuring these multi-point flow field properties across the range of hot and cold jet flows is required.

There is a large collection of flow statistics data on cold jets, where space-time correlations have been performed to estimate turbulent length and time scales [5,6]. However, cold jet flow data are not directly applicable to hot jet flows. The available data on heated jets is much more sparse. Ahuja, et al. used LDV to obtain single-point turbulence measurements in hot subsonic jets [7]. The only previous application of planar velocimetry techniques to acquire space-time correlations in hot jet flows was demonstrated by [2]. PIV has been previously used to obtain space-time correlations in a low speed water tunnel flow [8]. Multi-plane, stereo PIV has also been used to obtain space-time correlations in a low speed, cold, lobed nozzle flow [9].

PIV is able to provide high spatial resolution velocity measurements through the use of high resolution cameras. The temporal resolution has been limited by laser repetition rate and camera framing rate. The temporal limitations have previously been overcome by using two independent PIV systems, so that the location and time delay between image acquisitions could be varied without restrictions [2]. The complexity and difficulty of implementing such a dual PIV system is daunting. A kHz rate PIV system has previously been used to study the low frequency oscillations in shock induced turbulent separation [10]. In this work, the diode pumped Nd:YLF laser produced relatively long duration pulses, which in the high speed flow, yielded streaked particle images that decreased the accuracy of the velocity estimates. Commercial Temporally Resolved PIV systems are now available which support acquisition rates up to 1 kHz with laser pulse energies in the 20 mJ/pulse range. These systems are adequate for many non-stationary flows, but are incapable of providing relevant spectral properties of hot, turbulent jet flows.

A new Time Resolved PIV system has been developed and implemented at NASA GRC, which is capable of acquiring planes of flow measurements in supersonic jet flows at rates up to 20 kHz (frame pairs at 10 kHz) and time durations over 2 seconds, providing time records for computing spectral properties of the flow out to 5 kHz. The new TR-PIV system has been successfully applied to both hot and cold jet flows over a range of temperatures and Mach numbers in the SHJAR facility at NASA GRC. These measurements were obtained over an axial range of 0.5 to 12 diameters in both the shear layer and along the jet centerline. Measurements at the same Mach number for both cold and hot flows allows a direct comparison of the changes in the flow field properties. The cold flow measurements (T/T_∞ =0.89) obtained at Mach 0.5 using the new Time-Resolved PIV system are validated by comparison with previous hotwire anemometry measurements. Validating the TR-PIV measurements against well accepted hotwire results in the incompressible cold flow case ensures our confidence in the TR-PIV measurements in compressible, high temperature flows where hotwire measurements are not possible. The extensive time and spatial resolution of these measurements provides a new database of flow measurements previously unavailable. These flow measurements provide Lagrangian type measurements of the convective turbulent structures in the shear layer of an exhaust nozzle facilitating the computation of two-point space-time correlations. Two-point space-time correlation results for a Mach 0.9 flow case at both hot and cold conditions are presented illustrating the differences in the turbulent properties caused by temperature. This new database of flow measurements is being used to validate empirical correlations which predict the turbulent decay of the shear layer, a primary noise generation source. Examination of the actual two-point space-time correlations will guide the assumptions and flow models currently employed in aeroacoustic models.

II. Experimental Setup

A. SHJAR Facility

The Small Hot Jet Acoustic Rig (SHJAR) is a single-stream hot jet rig that can cover the range of Mach numbers up to Mach 2, and static temperature ratios up to 2.8 using a hydrogen combustor and central air compressor facilities. For most testing, SHJAR uses a 50.8 mm diameter nozzle, but can operate larger nozzles with some limitation on cold setpoints at high Mach number. The SHJAR is located within the AeroAcoustic Propulsion Laboratory (AAPL) at NASA GRC. The AAPL is a 65 foot radius geodesic dome with its interior covered by sound absorbent wedges that provide the anechoic environment required to study propulsion noise from several rigs that are located within. The jet rigs are positioned such that they exhaust out the open doorway, allowing the flows to be seeded with particulates and removing issues related to background noise from flow collectors. The nozzle being used in this test is one of a family of convergent nozzles, called the Simple Metal Chevron (SMC) nozzles, designed to be simple to characterize with similar dimensions such as inlet diameter (15.24mm), lip thickness (1.27mm), outside face angle (30° to jet axis), and parallel flow section at the exit (6.4mm). The facility has a 0.5m long settling chamber, which contains a series of screens located 18" upstream of the nozzle entrance to isolate the jet initial condition from small vagaries of the jet rig such as boundary layers. For this test, the SMC000 nozzle (no chevrons), with a diameter D=50.8 mm was used. Flow conditions from Mach 0.5 to 0.9 and temperature ratios of 0.89 and 2.7 were covered in the test matrix.

B. Flow Seeding

For PIV, the fluid motion being measured is marked by the use of particles. These particles must be sufficiently small so they will have no slip relative to the fluid (so that their motion is the same as the fluid motion). In addition, all fluid must be laden with particles at a concentration high enough that sufficient particles (5-10) are found in an interrogation region of the recorded PIV images. In these tests we are mixing two fluids: the core stream and the ambient. It is also crucial that the seed be fully mixed and dispersed in the flow before the measurement region in order to assure good quality PIV images. Finally, the seed must not be affected by the high temperatures of the gas; this is especially true of the seed in the core stream at 520 C.

Two independent seeding systems were required in this study. The hot nozzle flow was seeded with a refractory seed material and the ambient air was seeded using a commercial 'smoke' generator. The refractory seed material used for the jet flow was 0.5 μm diameter alumina powder. A dispersion of the alumina seed material in ethanol was prepared using a pH stabilization technique [11]. The alumina/ethanol dispersion was dispersed in the flow well upstream of the nozzle using an air-assisted atomizing nozzle. The pH stabilization technique provides highly dispersed, unagglomerated seed particles in the flow. The ambient fluid was seeded with 0.3 μm mineral oil droplets produced by a commercial smoke generator. A large room circulation fan was used to disperse the concentrated smoke emitted by the smoke generator, providing a low velocity, uniformly seeded ambient air around the research jet.

C. High Speed PIV System

Implementation of PIV measurement systems in the AAPL facility requires installation of the system on a large box beam traverse rig measuring 7x7x7 m in size, as seen in figure 1. This traverse has a range of roughly 2.5m along the jet axis with an accuracy of 1mm. The TR-PIV system implementation for this nozzle shear layer test represents an optimization of the available laser pulse energy and the flexibility afforded by the CMOS cameras to select a high aspect ratio region-of-interest at high framing rates. In order

to achieve the objective of measuring a long spatial extent of the nozzle shear layer flow, the TR-PIV system was configured so that the laser light sheet propagated along the jet axis. By using a pair of CMOS cameras mounted side by side at the nozzle lip line height, the axial extent of the flow field being imaged was maximized. Figure 2 shows the overlapped fields of view from the camera pair used to record the long axial extent of the shear layer flow. Forming the pulsed laser beam into a short height, thin laser light sheet ensured that there was sufficient energy density across the CMOS cameras' field of view so that the light scattered by the submicron sized seed particles in the flow could be detected. The laser head was mounted on a shelf on the right side of the rig and the laser power supplies were mounted on the floor next to the traverse, due to their large size and weight.

The CMOS cameras used in this study were Photron Ultima APX-RS cameras, which have 17.5 μm square pixels in a 1024x1024 pixel sensor. Each camera is capable of operating at 3000 fps at full resolution. Higher framing rates are available at reduced resolution. The objective of this test was to obtain Time Resolved PIV measurements of the flow at 10 kHz. In order to acquire "frame-straddle" image pairs at 10 kHz, the Photron cameras were operated at a framing rate of 20 kHz. In the remainder of the text, any reference to 10 kHz PIV implies that the cameras were operated at a frame rate of 20 kHz with the laser pulses synchronized to "frame straddle" the image frame pairs at 10 kHz. At 20 kHz, the sensor region of interest was set to 144x1024 pixels. The Photron APX-RS camera is a low noise design and has dynamic range of 10 bits, although only 8 bit image data was stored in these tests. The cameras were equipped with 85 mm focal length lenses with 1.4x teleconverters to obtain the desired 19 mm x 150 mm field of view from each camera at 20 kHz. The cameras were each equipped with 8 gigabytes of on board memory and a gigabit Ethernet interface for downloading the acquired image data. Each camera was connected to a separate PC to facilitate faster image downloads. Although the image acquisition time was slightly over 2.2 seconds, the image download time was typically 15-19 minutes/camera. The long download time is a limitation caused by a combination of the firmware used in the Photron cameras and the MS Windows operating system's inability to handle tens of thousands of files in a single directory. Registration of the camera images was obtained by aligning the camera fields of view with a ruler in the plane of the light sheet. The cameras were controlled by the 'FastCam' commercial software package provided by Photron.

The pulsed light sheet illumination was provided by a Quantronix Infini dual head laser system. The laser heads and beam combining optics are housed in a single enclosure. The Infini laser is lamp pumped and uses an RF driven Q-Switch to generate the 10 kHz pulses from each laser head. The nominal output pulse energy is 6 mJ/pulse/head at 10 kHz. The beam has an $M^2 < 16$ and the pulse length is 130 nsec at Full Width Half Maximum. The laser head is equipped with a remote shutter for turning off the laser output. The laser beam propagated downstream, parallel to the jet axis, to the light sheet forming optics as shown in figure 1. Pairs of cylindrical and spherical lenses were required in order to form the beam from the laser into a 20x2 mm light sheet at the measurement plane.

Two digital delay generators were used to control all of the system timing and synchronization. One delay generator was used to externally trigger the cameras, which needed to operate at 20 kHz in order to obtain image frame pairs at 10 kHz. The 20 kHz camera trigger signal was input into a second delay generator where it was used to synchronize the camera framing rate to the 10 kHz dual head laser pulse firing times. The cameras could have been used as a master time-base, however, during image saving operations the trigger output signal from the Photron cameras inverts in polarity and does not always provide a stable trigger source for the laser. Since laser failure can occur if a stable trigger signal is not supplied, the digital delay generator was used to provide continuous camera/laser timing signals.

The test matrix required measurements in both the shear layer and along the nozzle centerline in the potential core of the jet. Measuring the shear layer flow along the nozzle lip line necessitated propagating the laser light sheet from a downstream location back upstream to the nozzle exit. The light sheet was vertically centered on the nozzle lip line. The laser head was mounted so the beam propagated in a downstream direction. A 100x100 mm box beam was mounted on the large traverse to support the light sheet forming optics. The laser beam was turned 90° along the box beam, where the light sheet forming optics were mounted. The light sheet optics were enclosed in a sheet metal housing to protect them from the hot, seeded jet exhaust. A fused silica window was placed at the exit of the enclosure. A nitrogen purge stream of air was directed over the face of the exit window in order to keep it clear of seed material. In addition to the nitrogen purge, a right angle sheet metal wedge was fabricated to protect the exit window, see figure 3. The protective wedge had a slot cut out for the exiting laser beam and was flooded with 120 psi air to prevent seed material from entering the enclosure and coating the exit window. The laser beam propagated 2.1 m upstream from the sheet forming optics to the nozzle. For the measurements in the nozzle potential core, the light sheet generating optics and camera system were raised 25.4 mm and the laser beam propagated inside the nozzle.

Figure 3 shows the TR-PIV system in operation. The dual PIV computer systems were remotely located during data acquisition and controlled the CMOS cameras via their gigabit Ethernet interface. The dual TR-PIV camera system had an axial stream view against a black velvet covered background. The SHJAR is an outdoor facility, which typically dictates operation after sunset in order to avoid background

contamination by sunlight. However, due to the short exposure intervals when operating the CMOS cameras at 20 kHz, measurements were obtained in full daylight conditions, without interference filters.

III. Data Analysis

The collected TR-PIV image data were processed using an in-house developed PIV cross-correlation processing program called PIVPROC [12]. The correlation based processing software program supports subregion image shifting and multi-pass correlation in order to improve the spatial resolution of the resultant velocity vector maps. In addition, PIVPROC also supports subregion distortion processing [13], which proved to be critical in reducing the acquired image data. A detailed description of the data processing steps deemed necessary to extract the relevant flow field information can be found in [14]. The PIV images were processed using a first pass subregion size of 64x32 pixels, with 50% overlap, followed by 6 passes using 32x32 pixel subregions again with 50% overlap. Then two additional passes were computed using the subregion distortion technique. Hence, a total of 9 correlation passes were used on each data set. The resulting spatial resolution of the velocity vector grid was 0.05 D or 2.5 mm. At each measurement point, a total of 21845 image frame pairs were collected, per camera. Each measurement station in the flow survey contained 16 Gigabytes of image data (8 GB/camera).

The computed vector maps from each camera were then merged into a single velocity vector map, where the processing grids in each of the camera images was shifted to ensure proper meshing of the combined vector maps. Typically 5 grid points from each camera's individual vector map overlapped in the combined vector maps. The processed, merged velocity vector maps were then ensemble averaged while imposing hard velocity cutoff limits and Chauvenet's Criterion to remove statistical outliers from the time sequence records [15]. Any identified outliers were flagged so that they could be replaced in subsequent time domain processing. The sequence of velocity vector maps were then converted from planar spatial data to a 2-D spatial grid of time series measurements and written to a single time record file.

A. *Spectral Computations*

The time record file was read into the spectral processing program. Any data points that had been flagged in the spatial ensemble average processing (via hard velocity cutoff limits or the Chauvenet's Criteria) were replaced by interpolating across the missing point in the forward and backward time steps. Hence, spurious vectors identified in the ensemble average processing were replaced by a time-wise interpolated value. Replacement of any missing velocity vectors was required in order to ensure that a continuous time record was input to the spectral computation algorithm. Less than 1% of the vectors at any given grid point were replaced via temporal interpolation. Tests confirmed that vector replacements "in time" never exceeded more than one time step.

The ensemble averaged mean values of the reconstructed velocity time records were then computed at each grid point in the vector maps and subtracted from the velocity records to produce zero-mean velocity records. Spectral periodograms were then computed from the 21845 point (10 kHz) time records using 50% overlap and Welch windowing, in order to minimize the variance in the resulting periodograms. Assuming a total record length of $2 \cdot K \cdot M$ (where the total record is divided up into K segments of length $2M$ each), then by using 50% overlapping records the variance in the Power Spectral Density (PSD) estimate is reduced by the factor $9K/11$ [16]. The 21845 point time records were processed using 512 point periodograms in K=42 data segments.

The Hotwire data used for comparing the TR-PIV data were collected using a Dantec model 55p11 with a 5 μm diameter, 1.25mm long Platinum-plated tungsten wire. The hotwire was operated at an overheat of 0.6 and was controlled by a Dantec Streamline 90C10 module. The hotwire signal was digitized at 10 kHz and 16 bits resolution using an RC Electronics Datamax Digital Recorder. A 4 kHz anti-alias filter was used to filter the hotwire signal before it was digitized and stored. The 8 second long, 80,000 point hotwire time records were converted to zero mean flow records and 512 point periodograms were computed using Welch windows in K=78 data segments. The hotwire data were acquired several years previous to the current work with the objective of accurately characterizing the spread of the shear layer as a function of axial position. The conservative anti-alias filtering used to acquire the hotwire data may have removed too much of the high frequency content of the signal near the nozzle and therefore possibly under estimates the true turbulence intensity along the lip line near the nozzle exit. For range x/D > 1 the frequency content in the signals has dropped off significantly so that the hotwire turbulence estimates are more realistic.

B. *Two Point Statistics*

Our motivation for developing Temporally Resolved PIV is driven by acoustic theory, which requires knowledge of the two-point space time correlations of the velocity field. TR-PIV yields time records of velocity across a planar grid of measurement points, which directly lends itself to the computation of two-point space time statistics. The processed time record/vector maps were then processed to compute the two-point spatial-temporal correlations via:

$$R_{ij}(\vec{\xi}, t, \vec{x}) = \frac{\overline{u_i(\vec{x}, t) u_j(\vec{x} + \vec{\xi}, t + \tau)}}{\sqrt{u_i^2 u_j^2}} \qquad (1)$$

where $\vec{\xi}$ is the spatial lag variable and τ is the time lag variable in the correlation computation about the spatial point $\vec{x}$. The correlation has been normalized here by the reference variances: $\sqrt{u_i^2 u_j^2}$. The space time correlation R_{ij} can then be used to compute the spatial and temporal length scales of the flow.

VI. Results & Discussion

TR-PIV data were collected at 10 kHz in the Small Hot Jet Acoustic Rig fitted with the SMC000 50.8 mm diameter nozzle. Data were collected over a range of Mach numbers (0.5-0.9) and temperature ratios (T/T_∞=0.89 to 2.7). In addition, we have previous hotwire survey measurements from the SMC000 nozzle flow at Mach 0.5, which were used as a baseline case for validating the TR-PIV measurements. Figure 4 shows the SMC000 50.8 mm diameter nozzle and an instantaneous velocity vector map acquired at 10 kHz, which illustrates the spatial resolution of the measurements. The vector field shown here is the result of merging the left and right camera processed vector maps. Both high speed packets of fluid from the nozzle core flow and low speed fluid packets from the ambient are observed in the instantaneous vector field.

The "quality" of the ensemble averaged data sets is determined by examining the number of good velocity measurements at each grid point in the velocity vector map. Spurious velocity vectors are removed during the ensemble averaging process as described above. The data quality is defined as the number of good data points at each grid point relative to the total number of measurements in the ensemble. High data quality is typically obtained via a uniformly dispersed, high concentration flow seeding.

Ensemble averages of the TR-PIV data sets were computed in order to evaluate the flow field properties and ensure accurate processing of the data. Figure 5 shows the mean velocity, turbulence intensity and data "quality" resulting from the PIV processing. The mean velocity field appears unremarkable, the bottom edge of the high speed nozzle core is observed at the top of the flow field and the entrainment of low speed ambient air is observed at the bottom edge of the flow field. The relative standard deviation in the u-component of velocity is defined here as σ_u/U_{id}, where U_{id} is the ideally expanded jet velocity computed using the plenum pressure. Axial turbulence intensities of approximately 12% are observed at an x/D of 1, which exactly match the hotwire measurements at this axial location. The data quality is better than 98% throughout the entire flow field. The axial turbulence levels in the shear layer at x/D=0.5 are slightly higher than expected, which is attributed to the large velocity gradients that can bias the velocity estimates depending on the magnitude of the gradient relative to the size of the correlation subregion. Further downstream, x/D > 0.7, the subregion distortion technique is able to correct for the large velocity gradients and the turbulence levels are in agreement with the hotwire results.

PSDs for the TR-PIV data are shown in figure 6a and b along with hotwire PSDs at a radial location on the nozzle lip line (y/D=-0.5) and at axial locations of x/D=2 and x/D=3. The hotwire spectra have a lower variance than the TR-PIV spectra due to both the application of anti-alias filtering and the larger number of data segments (K=78, vs. K=42 for TR-PIV) averaged together to compute the periodogram. The TR-PIV data were smoothed using a 5 point moving average filter. The TR-PIV data lie nearly on top of the hotwire spectra for the range of 1 kHz and above. Below 1 kHz there are some slight deviations between the TR-PIV data and the hotwire spectra. The high frequency dogleg in the PIV spectra is a result of aliasing in the acquired PIV data [14].

A. TR-PIV versus Hotwire

Radial surveys at the nozzle centerline were taken using a hotwire probe at axial planes from 0.2 to 10.0 diameters downstream from the nozzle exit. The hotwire probe was mounted on a horizontal translation stage within the large blue traverse rig used to translate the PIV system shown in figure 1. The surveys were obtained at y/D increments of 2.5. Figure 7a contains line profiles of the relative standard deviation in the u-component of velocity normalized by the ideally expanded jet velocity U_{id} as measured by the hotwire probe for axial locations of 0.2, 0.5, 0.7, 1.4 and 2.0 nozzle diameters. These surveys only show one-half of the nozzle radial survey plane. The relative turbulence in the axial velocity along the lip line ranges from σ_u/U_{id} = 0.05 at x/D=0.2 to σ_u/U_{id} = 0.14 at x/D=2.0. The hotwire profiles indicate that the shear layer migrates slightly away from the nozzle centerline at increasing axial locations. The TR-PIV measurement results are shown in figure 7b. The TR-PIV camera was not positioned right at the exit of the nozzle in order to keep unwanted flare light from the nozzle lip from reaching the camera. Hence, only TR-PIV axial profiles of σ_u/U_{id} at y/D planes from 0.7 to 2.0 are plotted here for comparison to the hotwire measurements. The TR-PIV measurements at x/D=0.7 are slightly corrupted due to edge effects in the processed velocity vector maps. Hence, the x/D=0.7 PIV profile is slightly higher than the corresponding hotwire profile. The TR-PIV profiles are nominally at the same level or slightly higher (0.15%) than the hotwire measurements. This is not unexpected since the TR-PIV data are aliased due to the lack of an anti-aliasing filter. The TR-PIV profiles appear to be narrower than the hotwire profiles and also appear to remain relatively centered along the nozzle lip line at increasing axial locations.

In all of the analyses above, we have focused on the nozzle lip line. It is also constructive to compare the spectral surveys obtained using the hotwire against the TR-PIV results over the remainder of the radial extent of the flow. Figure 8a shows

the hotwire survey planes plotted at three x/D planes (5, 7, 10) versus survey location y/D versus frequency in Hz. In figure 8b the TR-PIV data at x/D=5 are overlaid on the hotwire data. The TR-PIV measurements very closely match the hotwire measurements in magnitude and spatial extent, both along the lip line and over the radial extent of the PIV system field of view. The agreement between the TR-PIV and the hotwire measurements are nearly identical at x/D = 7 and 10. Note that we have only shown a single line from the TR-PIV data set. The TR-PIV results contain a nearly continuous block of y/D surveys from x/D=0.5 out to x/D=6 for a singe axial measurement station. TR-PIV measurements were acquired at several overlapping axial stations, yielding a continuous 2-D map of flow spectra from x/D=0.5 to x/D=12.

B. TWO-POINT STATISTICS

The correlation of the axial velocity in the axial direction, as defined by equation 1 defines $R_{uu}(\xi,\tau)$ as the element in the correlation tensor that we are computing. The axial velocity space-time correlations were computed at the reference locations x/D = 3 and 12 and at y/D = -0.5 for the TR-PIV data at the Mach 0.9 flow condition and at the temperature ratios: T/T_∞=0.89 and 1.76. Spatial shifts in the axial direction are denoted ξ_x and spatial shifts in the radial direction are denoted ξ_y. Figure 9a-d shows the axial velocity correlation $R_{uu}(\xi,\tau)$ for the two temperature ratios at the $\xi_y = 0$ plane (zero radial shift), where the vertical axis is dimensionless time lag, τ, scaled by the convective velocity U_c and the nozzle diameter and the horizontal axis is the dimensionless spatial shift ξ_x/D. The correlation function starts out at unity amplitude at zero time (τ=0) and space (ξ_x=0) shifts and then clearly delineates the decay of the turbulence in the jet flow, via the decreasing amplitude of the correlation peak and the broadening of the spatial extent of the turbulence. The slope of the correlation function is directly proportional to the convection velocity, which for the T/T_∞=0.89 case is 195 m/s at x/D=3 and 143 m/s at x/D=12; and for the T/T_∞=1.76 case is 171 m/s at x/D=3 and 117 m/s at x/D=12. The reduction in the convection velocity for the hot flow case is caused by the higher momentum of the colder ambient flow, which through mixing inside the shear layer, is pulling down the amplitude of the core jet velocity. At x/D =3, the correlation length is fairly short and there appears to be no significant difference between the cold and hot cases. At x/D=12, the hot flow case shows a faster growth rate of turbulent structures, as indicated by the width of the correlation function. In both cases at x/D=12, the convective velocity is decreasing at long time and spatial delays, as indicated by the upward curving of the correlation function contours. The quality of the TR-PIV data records is verified by the clearly defined correlation function even at these locations very close to the jet where the turbulence structures are just beginning to develop.

V. CONCLUSIONS

Measurement of space-time correlations in both hot and cold jet flows is now possible due to the development of a Temporally Resolved PIV system. Using the TR-PIV system to capture a long (6 jet diameters) spatial extent of the nozzle shear layer provides simultaneous spatial and temporal maps of the flow field properties. Application of TR-PIV in a Mach 0.5 jet flow revealed turbulent structures which were clearly observed to advect downstream in animations of the long vector map sequences. The high quality, high spatial resolution velocity vector maps are attributed to the high quality, uniformly dispersed flow seeding and through the use of advanced PIV data processing strategies such as subregion distortion.

TR-PIV time records were acquired at 20 kHz, yielding processed, planar flow measurement time records at 10 kHz. The planar velocity time records were used to compute flow spectra at all points across the processed PIV velocity vector maps. The TR-PIV spectra and turbulence estimates were then compared with those obtained using hotwire anemometry. The TR-PIV results exactly match the nominally 1% accurate hotwire results for x/D > 1. For x/D < 1, the TR-PIV turbulence estimates were higher than the hotwire results due to: 1) the low sampling rate (10 kHz) and very conservative anti-aliasing filter setting (4 kHz) used to acquire the hotwire data prematurely truncated the hotwire spectra resulting in under-estimated turbulence levels in the region x/D < 1; and 2) as a direct consequence of aliasing of higher frequencies in the flow down into the measured frequency bands in the TR-PIV data. The TR-PIV results showed a narrower shear layer and constant propagation trajectory compared to the hotwire results which showed a larger spread angle and a shear layer that propagated off of the nozzle lip line. Validating the TR-PIV results in a Mach 0.5 cold flow against hotwire measurements establishes the credibility of the TR-PIV technique and the additional flow measurements obtained in compressible flows at elevated temperatures.

In addition to validating the TR-PIV measurements with hotwire anemometry, two-point space-time correlations were computed for the Mach 0.9 flow case at x/D=3 and x/D=12 for both hot and cold flow cases. The space-time correlations indicated that increasing the temperature appears to increase the growth rate of the turbulent structures. Much work still needs to be done to process and examine these time-resolved flow measurement records in order to accurately characterize the turbulence decay in jet flows. The results obtained from these further analyses are being used to verify/modify the current assumptions and models used in Computational AeroAcoustic (CAA) codes.

ACKNOWLEDGEMENT

The author would like to thank Ray Loew and Dennis Eck for their support in the operation of the SHJAR facility and also thank W. Trevor John and Garret Clayo for their assistance in the setup and installation of the TR-PIV system. Discussions with Dr. James Bridges were also invaluable in interpreting some of the results.

REFERENCES

[1] Wernet, M. P. and Bridges, J., "Application of DPIV to Enhanced Mixing Heated Nozzle Flows," AIAA 2002-00691, 40th Aerospace Sciences Meeting, Reno, NV 2002.

[2] Bridges, J. and Wernet, M. P., "Measurements of the Aeroacoustic Sound Source in Hot Jets" AIAA-2003-3130, 9th AIAA/CEAS Aeroacoustics Conference, 2003.

[3] Lighthill, M. J., "On Sound Generated Aerodynamically, I. General theory," Proc. Royal Soc. London A, 211, 564-587, 1952.

[4] Seiner, J. M., Ukeiley, L. S., Ponton, M. K., and Jansen, B.J., "Progress in Experimental Measure of Turbulent Flow for Aeroacoustics," AIAA 2002-2402, AIAA/CEAS Aeroacoustics Conference, 2002.

[5] Chu, W. T., "Turbulence Measurements Relevant to Jet Noise," Univ. Toronto Institute for Aerospace Studies, UTIAS Report 119, 1966.

[6] Laurence, J. R., "Intensity, Scale, and Spectra of Turbulence in Mixing Region of Free Subsonic Jet," NACA Report 1292, 1956.

[7] Ahuja, K. K., Lepicovsky, J., Tam, C.K.W., Morris, P.J., and Burrin, R.H., "Tone-Excited Jet: Theory and Experiments," NASA CR-3538, 1982.

[8] Oakley, T. R., Loth, E., Adrian, R. J., "Cinematic Particle Image Velocimetry of High-Reynolds-Number Turbulent Free-Shear Layer," AIAA Journal 34(2), pp. 299-308, 1996.

[9] Hu, H., Saga, T., Kobayashi, T., Taniguchi, N., Yasuki, M., "Dual-Plane Stereoscopic Particle Image Velocimetry: System Setup and its Application on a Lobed Jet Mixing Flow," *Exper. In Fluids*, **31**, pp. 277-293, 2001.

[10] Bueno, P. C., Ganapathisubramani, B., Clemens, N. T., and Dolling, D. S., "Cinemagraphic Planar Imaging of a Mach 2 Shock Wave/Turbulent Boundary Layer Interaction", AIAA-2005-0441, 43rd Aerospace Sciences Meeting, Reno, NV, 2005.

[11] Wernet, J. H. and Wernet, M. P., "Stabilized Alumina/Ethanol Colloidal Dispersion for Seeding High Temperature Air Flows," *Proceedings of the ASME Symposium on Laser Anemometry: Advances and Applications,* Lake Tahoe, NV, 1994.

[12] Wernet, M. P., "Fuzzy Logic Enhanced Digital PIV Processing Software," *Proceedings of the 18th International Congress on Instrumentation for Aerospace Simulation Facilities (ICIASF),* Toulouse, France, June, 1999.

[13] Gui, L., Werely, S.T., "A Correlation-Based Continuous Window-Shift Technique to Reduce The Peak-Locking Effect in Digital PIV Image Evaluation", *Exper. In Fluids*, **32**, pp. 506–517, 2002.

[14] Wernet, M. P., "Temporally-Resolved PIV for Space-Time Correlations in Both Cold and Hot Jet Flows", Meas. Sci. Technol., 18 pp. 1387-1403, 2007.

[15] Taylor, J. R., An Introduction to Error Analysis, University Science Books, Oxford University Press, Mill Valley, CA., 1982.

[16] Welch, P. D., *Modern Spectrum Analysis* (New York: IEEE Press), Childers, D.G. (ed.), 1978

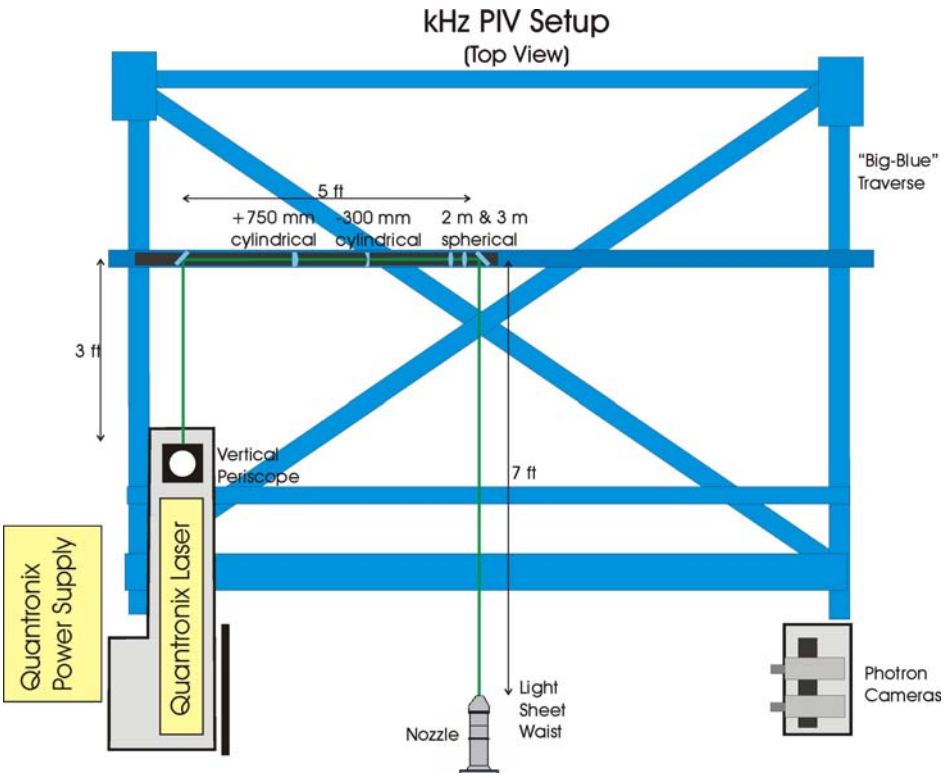

Figure 1: Schematic layout of kHz PIV system in the Small Hot Jet Acoustic Rig.

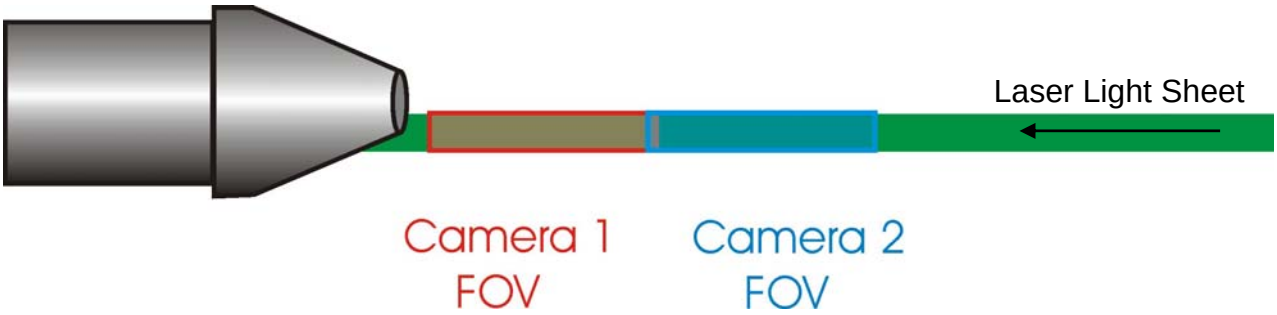

Figure 2: Illustration showing the laser sheet propagation upstream to the nozzle and the overlapping field of views from the two side-by-side Photron cameras.

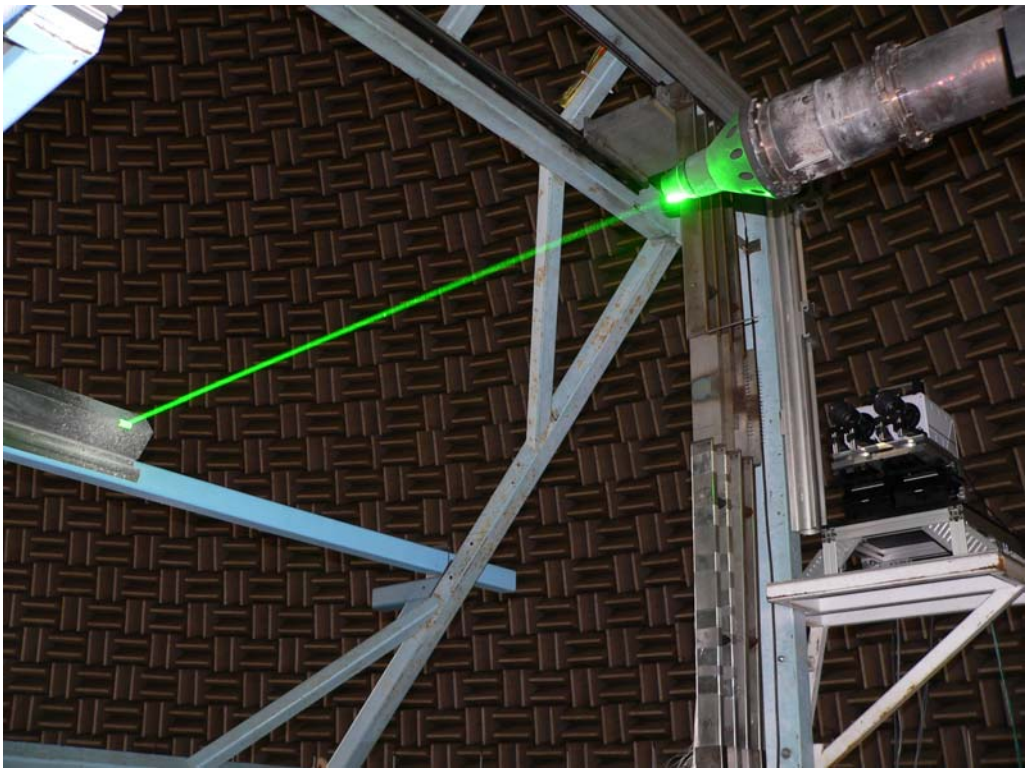

Figure 3: Picture of the setup in the SHJAR facility showing the cover over the light sheet forming optics, the light sheet impinging on the nozzle lip and the two Photron cameras.

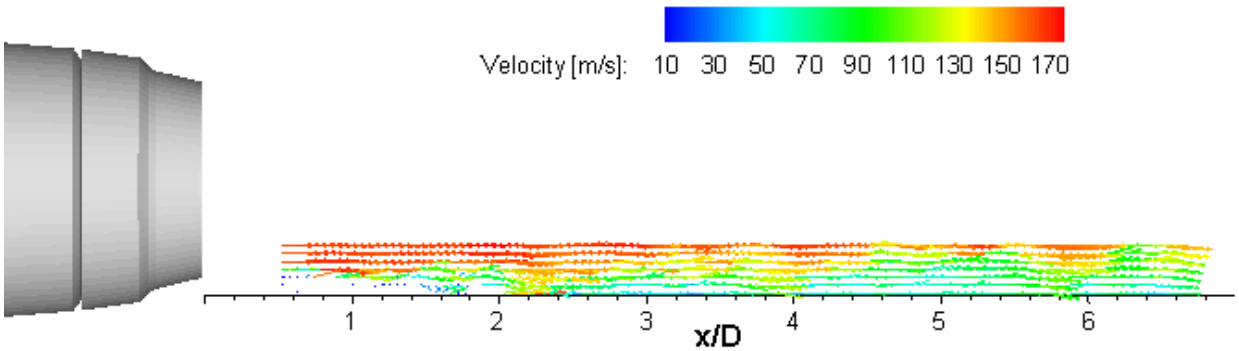

Figure 4: A single velocity vector map from the TR-PIV setup which illustrates the location of the measurements relative to the nozzle and the spatial resolution of the results.

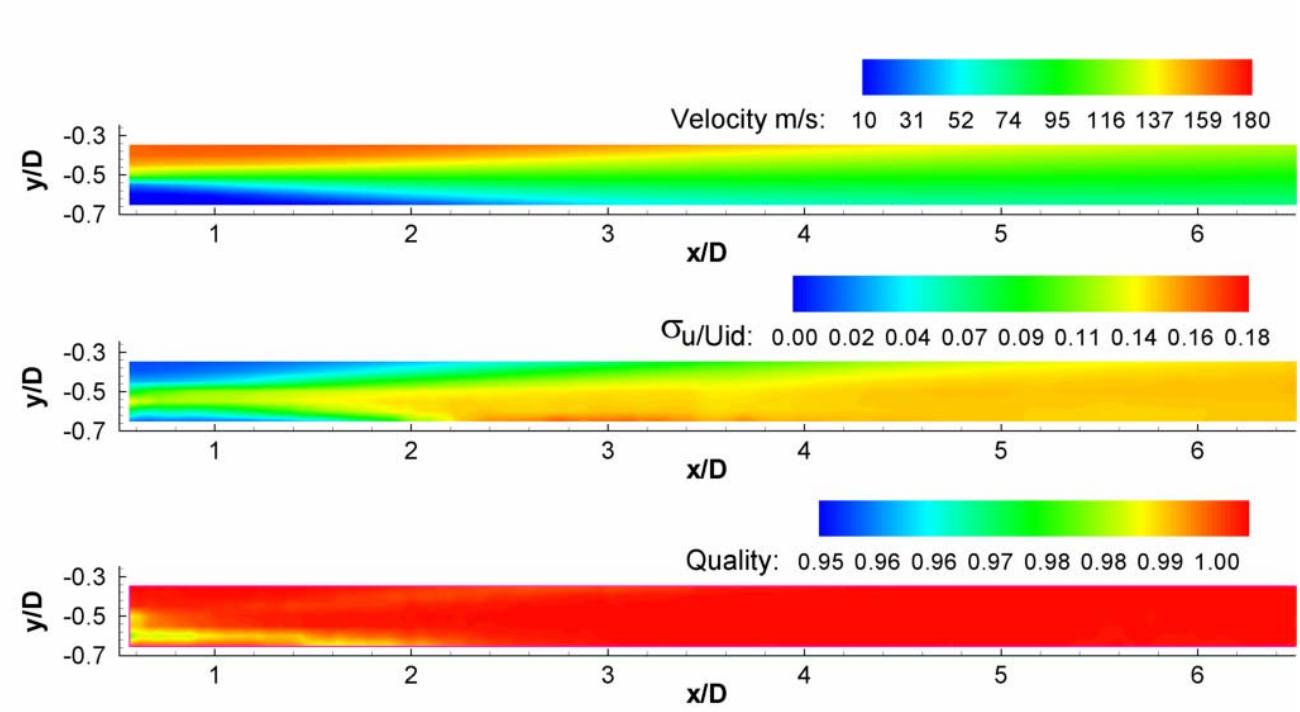

Figure 5: Ensemble averaged flow field showing velocity, σ_u/U_{id} and data quality for the TR-PIV. The axial turbulence intensity, σ_u/U_{id}, is very close to the expected turbulence levels in a Mach 0.5 jet flow. The data quality are high throughout the measurement region.

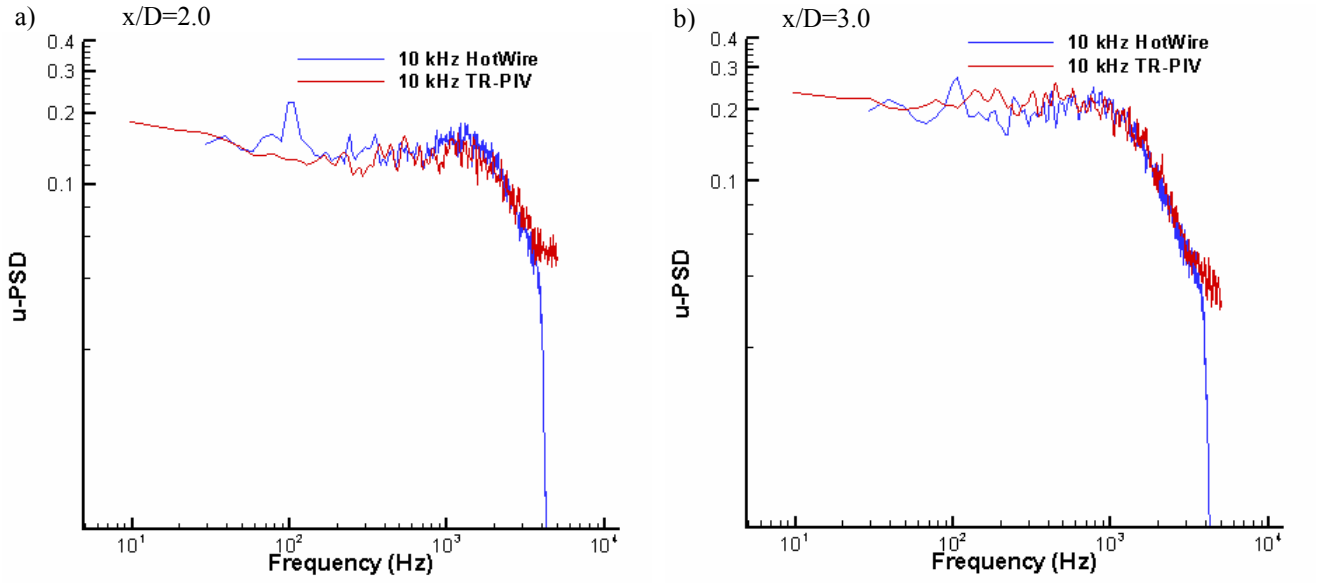

Figure 6: Comparison of TR-PIV Power Spectral Densities with hotwire PSDs for :a) x/D=2 and b) x/D=3. A 5-point moving average has been used to smooth the TR-PIV results.

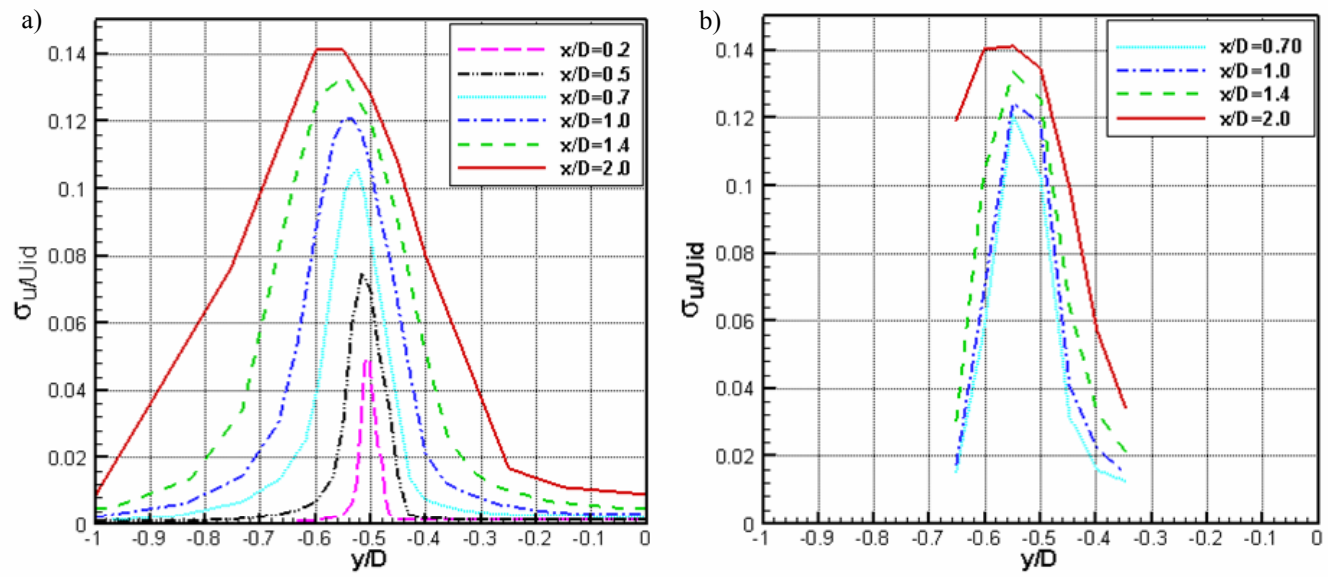

Figure 7: a) Hotwire surveys of σ_u/U_{id} at increasing axial distance from the nozzle; b) TR-PIV profiles of σ_u/U_{id} which are narrower then the hotwire profiles and remain centered on the nozzle lip line.

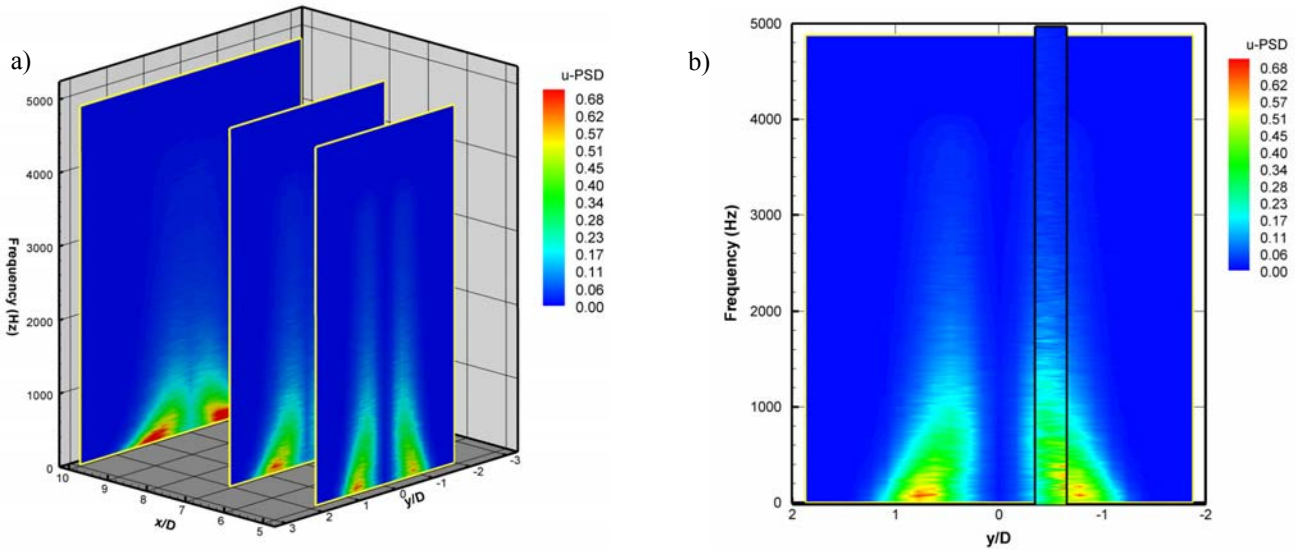

Figure 8: a) Hotwire radial surveys showing computed spectra; b) TR-PIV results overlaid on hotwire survey at x/D=5. The TR-PIV results very closely match the hotwire results even off of the nozzle lip line at x/D=5 and at survey planes further downstream.

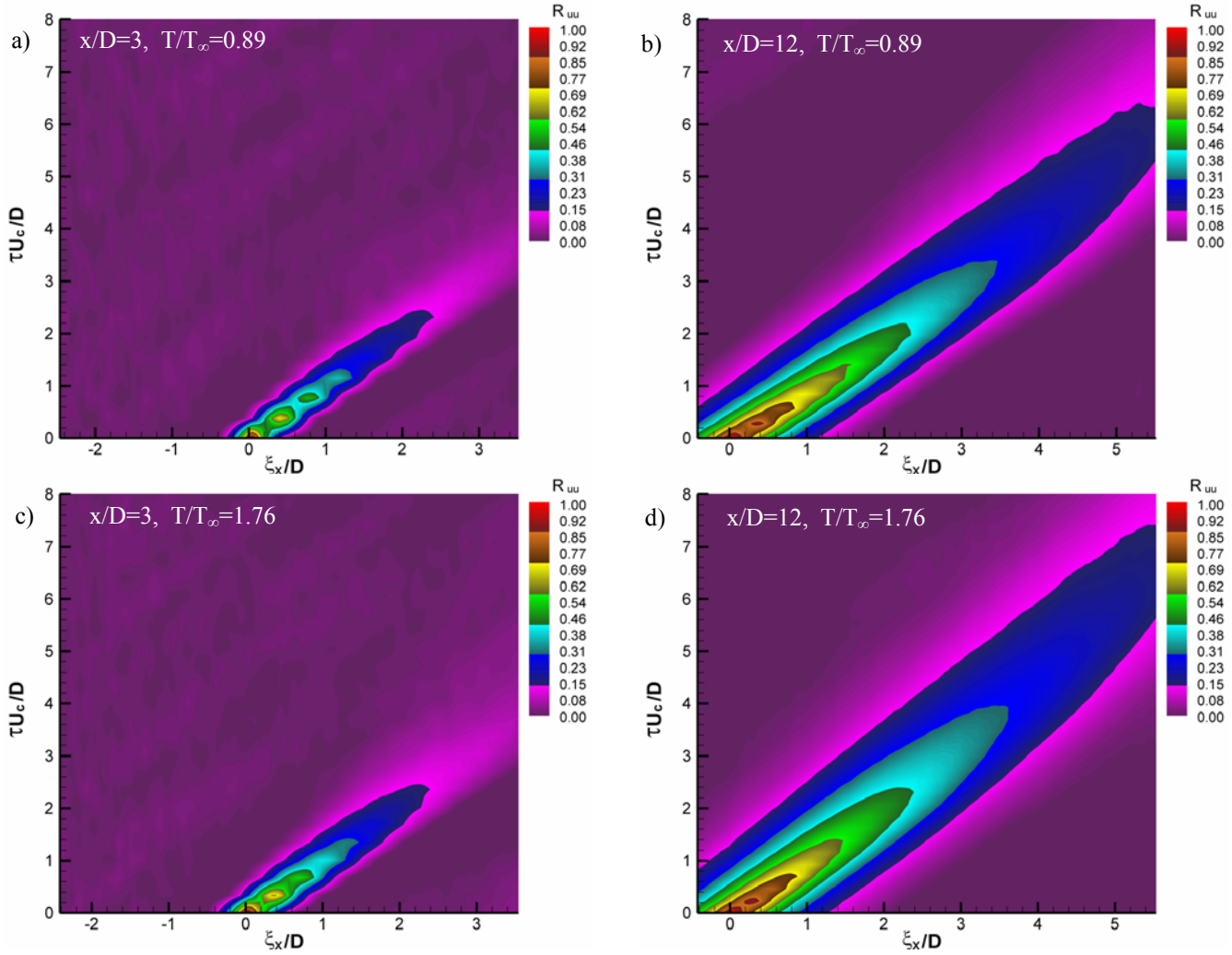

Figure 9: Space-Time correlations R_{uu} computed at x/D =3 & 12 and y/D=-0.5 for the Mach 0.9 flow case: a) and b) cold flow: T/T_∞=0.89; c) and d) hot flow: T/T_∞=1.76. At x/D=3, the correlations start at unity and decrease very quickly and spreads out due to the flow turbulence. For the hot flow cases the convective velocity is slightly lower and the correlation lengths are longer than the cold flow case. At x/D=12, the turbulent structures are growing as they convect downstream - as indicated by the wider spread in the correlation function.